Research Square

Preprints are preliminary reports that have not undergone peer review.
They should not be considered conclusive, used to inform clinical practice,
or referenced by the media as validated information.

Evolution Mechanism of Seepage-Induced Sand Inrush in Broken Rock Masses under the Coupled Effects of Particle Gradation and Outlet Boundary Conditions

Zhibin Lin
Henan Polytechnic University
zhaoyang Feng
Henan Polytechnic University
boyang zhang
zhangboyang@hpu.edu.cn
Henan Polytechnic University
yanchao wang
Henan Polytechnic University

Research Article

Keywords: broken rock mass, Talbot gradation, outlet boundary, permeable-plate aperture, particle migration, clogging instability

Posted Date: November 3rd, 2026

DOI: https://doi.org/10.21203/rs.3.rs-10917204/v1

License: This work is licensed under a Creative Commons Attribution 4.0 International License.
Read Full License

Evolution Mechanism of Seepage-Induced Sand Inrush in Broken Rock Masses under the Coupled Effects of Particle Gradation and Outlet Boundary Conditions

Zhibin Lin, Zhaoyang Feng, Boyang Zhang *, Yanchao Wang

School of Civil Engineering, Henan Polytechnic University, Jiaozuo 454000, Henan, China

* Corresponding author at: School of Civil Engineering, Henan Polytechnic University, Jiaozuo 454000, Henan, China.

E-mail addresses: linzhibin@hpu.edu.cn (Z. Lin), 212408020059@home.hpu.edu.cn (Z. Feng), zhangboyang@hpu.edu.cn (B. Zhang), 212308020022@home.hpu.edu.cn (Y. Wang).

Abstract

To elucidate the mechanism of seepage-induced sand inrush in broken rock masses under the coupled effects of particle gradation and outlet boundary, the seepage-induced sand inrush tests of broken rock mass under different Talbot gradation and permeable-plate aperture combinations were carried out with broken mudstone and aeolian sand as test materials. The variation rules of equivalent permeability, total sand discharge and the time to first sand emergence were analyzed. On this basis, the seepage-induced sand inrush mode and mechanism of broken rock mass were discussed in combination with experimental phenomena. The results show that : (1) With the increase of Talbot exponent or permeable-plate aperture, the equivalent permeability of broken rock mass shows a nonlinear growth trend, with an increase of 46.3 % -125.4 % and 106.4 % -182.3 %, respectively. (2) With the increase of Talbot exponent or the aperture of permeable plate, the total sand discharge in broken rock mass increases, and the time to first sand emergence is shortened. The total sand discharge increased by 410.0 % ~ 1366.7 % and 259.5 % ~ 994.5 %, respectively. (3) The seepage-induced sand inrush mode of broken rock mass can be divided into three types : Type I migration–deposition–clogging–slow-release mode with limited fine particle migration, Type II local clogging–staged release mode with fine particle stage release due to local instability of clogging structure, and Type III channel connectivity–sustained sand-discharge mode with local clogging difficult to form and rapid penetration of seepage channel.(4) Particle gradation affects particle filling and local clogging by regulating the content of the small-particle fraction (<0.8 mm) in the broken mudstone and the pore-filling capacity, whereas the outlet aperture regulates particle migration and channel formation through sieving constraints and outlet release conditions. Their coupled effects jointly alter the competitive relationship between local filling–clogging effects and outlet release capacity, causing the sand-inrush mode to progressively evolve from stable local clogging (Type I) to staged breakthrough (Type II) and sustained connectivity of dominant channels (Type III). The results can provide an experimental basis for risk identification and differentiated prevention and control of water–sand inrush in shallow coal seams.

Highlights

- Talbot gradation and outlet aperture jointly control seepage-induced sand inrush in broken rock masses.
- Equivalent permeability and total sand discharge increase with increasing Talbot exponent and outlet aperture.
- Three seepage-induced sand-inrush modes evolve from stable clogging to sustained channel connectivity.

• Mode transition is governed by the competition between fine-particle clogging capacity and outlet release capacity.

Keywords broken rock mass · Talbot gradation · outlet boundary · permeable-plate aperture · particle migration · clogging instability

1 Introduction

Thin bedrock, thick unconsolidated strata, and multiple aquifers are widespread in shallow coal seam mining areas in western China. Under the action of high-intensity mining, the caving zone and water-conducting fracture zone can readily connect with overlying unconsolidated aquifers, forming a water-sand migration channel and inducing roof water-sand inrush disaster [1-3]. For example, during mining of Working Face 22402 in Halagou Coal Mine, the overlying rock breaks to form a penetrating fracture network, which gradually evolves into a preferential water–sand migration channel under the action of high water head pressure. After the working face advances 38 m, water and sand inrush occurs and causes surface subsidence [4]; due to the large-scale pore structure formed by the joint recharge of multi-aquifer and the breaking of thin bedrock in Zhaogu No.1 Coal Mine, the risk of roof water and sand inrush is prominent and it is difficult to stop by itself [5]; in addition, the thin bedrock roof working face may also be complicated by roof cutting, which aggravates the degree of damage [6]. The above disasters show that the pore structure inside the broken bedrock and the boundary conditions of the outlet jointly affect the evolution process of water sand migration and sand inrush. Among them, the internal structural characteristics such as porosity, connectivity and particle gradation affect the migration conditions of particles and the development of seepage channels, while the boundary conditions such as water pressure, outlet aperture and discharge capacity further regulate the hydraulic action and particle release process. Therefore, it is of great theoretical significance and engineering value to study the evolution law and coupling mechanism of seepage-induced sand inrush in broken rock mass under different particle gradation and outlet boundary conditions.

Aiming at the problem of water-sand two-phase flow and sand-inrush disaster in broken rock mass, domestic and foreign scholars have carried out a lot of research on particle gradation, internal structure evolution and outlet boundary constraints. In terms of particle gradation and internal structure effect, Zhang et al. [7] used Talbot continuous gradation formula to prepare broken sandstone samples with different particle size ratios. It was found that the seepage process of water and sand can be divided into three stages : initial fluctuation, relative stability and attenuation, and the permeability and sand content increased significantly with the increase of porosity and Talbot exponent. For the fault fracture zone, the Talbot exponent, stone content and confining pressure will significantly affect the pore connectivity and the formation of dominant seepage channels [8]. Further research shows that particle loss will dynamically change the pore structure and accelerate the evolution of seepage, and promote the system to change from steady seepage to sudden increase seepage or even approximate pipe flow [9]. Numerical simulation also confirms that the continuous migration and loss of small particles is an important cause of variable mass seepage in fault zones [10].In addition, internal erosion and piping studies reveal the dual roles of small particle size components : fine particle content, particle size ratio and microstructure characteristics significantly affect erosion initiation conditions and permeability evolution [11-13]. Small particles may not only block the throat and inhibit channel connectivity through local filling and ' bridging ', but also participate in continuous loss and channel expansion as a preferential migration phase, thus aggravating the sand inrush disaster. In

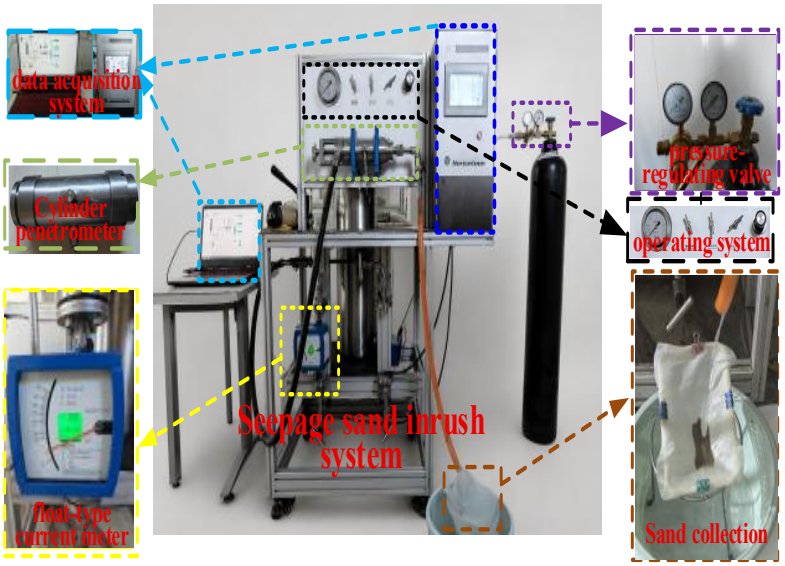
terms of the effect of outlet boundary and confined space, the fracture water-sand two-phase flow test shows that the fracture geometry, boundary pressure, particle size and concentration significantly affect the flow state and sand inrush risk of water-sand mixture [14-15]; the whole process of water and sand inrush is usually manifested as the stages of start-up, continuous outburst, siltation, clogging and balance [16]. The effective aperture of the fracture, the thickness of the sand layer and the particle properties jointly affect the particle migration process and the water-sand mass flow rate [17]; in confined space, water pressure and channel geometry will change the sorting, migration and accumulation mode of broken particles, and the clogging process shows obvious stage and boundary sensitivity [18].

In summary, the existing research has deepened the understanding of the seepage-induced sand inrush process of broken rock mass from the perspectives of particle gradation, internal structure evolution and outlet boundary constraints. However, the research on the coupling effect of particle gradation and outlet boundary is still insufficient. In particular, the migration, clogging and continuous sand inrush evolution of small-particle fraction below 0.8 mm under different gradation conditions in different outlet boundaries (such as the discharge capacity characterized by the pore size of the permeable plate) have not been systematically revealed. This restricts the theoretical leap from " single factor analysis " to " multi-factor coupling mechanism " of water and sand inrush disasters, and also constitutes the main starting point of this paper. Therefore, broken mudstone particles were used to prepare specimens with different Talbot gradations, uses the Talbot formula to prepare different particle gradation samples, combines different permeable-plate apertures to construct differentiated water-out sand-out boundary conditions, and carries out the seepage-induced sand-inrush test of broken rock mass. By analyzing the influence of Talbot exponent and outlet boundary change on equivalent permeability, total sand discharge and time to first sand emergence, the response mode and evolution mechanism of seepage-induced sand inrush of broken rock mass under the coupling effect of particle gradation and outlet boundary are discussed. The research results can provide experimental basis for the mechanism understanding and engineering prevention and control of water and sand inrush disaster in broken rock mass.

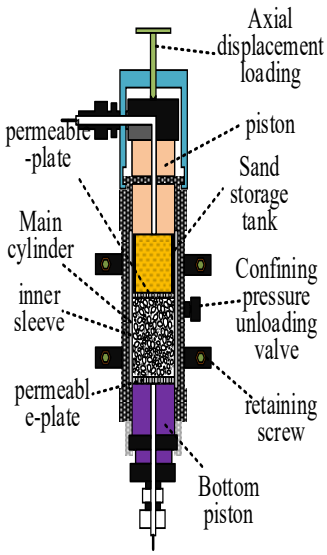
2 Experimental design for seepage-induced sand-inrush tests on broken rock masses

2.1 Test system

The test system for seepage-induced sand inrush in broken rock masses (Fig. 1) consisted of water and sand seepage system, seepage test device, data acquisition system and sand collection system. The water sand seepage system is composed of water storage tank, high pressure nitrogen bottle, pressure regulating device and hydraulic stabilizing device. It is mainly used to provide stable and controllable seepage power and ensure the continuity and stability of water pressure loading during the test. The seepage test apparatus realizes the simulation of different pore structures and seepage channel conditions by adjusting the sample size and axial displacement. The data acquisition system is used to monitor and record the pressure, flow and other parameters in the test process in real time. The sand collection system is used to collect and count the outflow particles to characterize the sand-inrush intensity and evolution characteristics. The system can better meet the requirements of water pressure loading, channel regulation, process monitoring and particle collection in the seepage-induced sand inrush test of broken rock mass.



（a）Seepage-induced sand-inrush apparatus for broken rock mass



（b）Structural diagram of the cylinder permeameter

Fig.1 Seepage-induced sand inrush test system of broken rock mass

2.2 Test scheme design

2.2.1 Test materials

The test uses different particle sizes of broken mudstone particles and aeolian sand as test materials, as shown in Figure 2. The original mudstone was crushed by a precision jaw crusher and screened to prepare five particle-size groups of <0.8 mm, 0.8-3 mm mm, 0.8-3 mm, 3-5 mm, 5-8 mm and 8-10 mm. Among them, considering that the small-particle fraction below 0.8 mm may have an important impact on local channel formation and sand burst response [19-21], the particles below 0.8 mm are defined as small particle size components in the gradation, 8 ~ 10 mm is the maximum particle size group, and the maximum particle size is controlled within 1 / 5 [22-23] of the inner diameter of the permeameter cylinder to reduce the boundary size effect and ensure the representativeness of the sample particle skeleton. The particles of each particle size were cleaned, dried and graded before the test to reduce the interference of water content and attached powder on the test results.



(a) Mudstone particles below 0.8 mm



(b) 0.8 ~ 3mm mudstone particles



(c) 3 ~ 5mm mudstone particles







(d) 5~8mm mudstone particles (e) 8~10mm mudstone particles (f) eolian sand

Fig.2 Materials used in the seepage-induced sand-inrush tests

2.2.2 Test variables and parameter combinations

(1) Talbot gradation of sample particles

To construct broken-rock specimens with different proportions of coarse and fine particles, the Talbot continuous gradation formula [24] was used to design the particle gradation of the mudstone. When the Talbot exponent $n$is relatively low, the mudstone specimens contain a higher proportion of fine particles, resulting in a stronger filling effect within the pores of the coarse-particle skeleton. As $n$increases, the particle gradation shifts toward coarser fractions, the content of fine particles smaller than 0.8 mm decreases, and the pore-filling effect is correspondingly weakened.

$$\frac{d}{D} = \left(\frac{P}{100\%}\right)^{\frac{1}{n}} \tag{1}$$

In the formula: d is a certain particle size; d is the maximum particle size; p is the cumulative mass percentage of particles less than particle size d; n is the Talbot exponent, which reflects the composition ratio of coarse and fine particles.

Combined with the previous grading calculation results and the sample filling characteristics [25-26], this paper selects n = 1.0,1.2,1.4,1.6,1.8 and 2.0 six groups of Talbot gradation conditions [27]. The total mass of the sample is uniformly controlled to 160 g, and the particle mass corresponding to each group of grading is shown in table 1.

Table 1 Mass distribution among particle-size ranges for different Talbot exponents

Talbot exponent	Particle mass (g)				
n	<0.8	0.8-3	3~5	5~8	8~10
1	12.8	35.2	32	48	32
1.2	7.7	30.4	32	52.8	37.1
1.4	4.7	25.6	30.4	56	43.3
1.6	3.2	20.8	28.8	59.2	48
1.8	1.7	16.6	27.6	61.1	53
2.0	1.0	13.4	25.6	62.4	57.6

（2）Outlet boundary size

In order to systematically study the influence of control conditions at the outlet end on the seepage-induced sand inrush behavior of broken rock mass, this paper sets different pore size permeable plates as the outlet boundary of the sample, as shown in Fig.4. The apertures of the permeable plate are 1 mm, 2 mm, 3 mm, 4 mm and 5 mm, respectively, forming five grades from small to large to reflect the differences in particle penetration, interception and clogging behavior under different outlet boundary constraints.



(a)1mm (b)2mm (c) 3mm



(d)4mm (e)5mm

Fig.4 Different aperture permeable plate outlet size

A two-factor test design was adopted, with Talbot exponent n and permeable-plate aperture d as the variables, and the specific parameter combination is shown in table 2. Thirty groups of test combinations were set up for six kinds of Talbot exponent and five kinds of permeable-plate aperture combinations, and each group of test combinations was repeated three times. Finally, the average value of the three test results was used as the representative value of the combination.

Table 2 Test grouping and variable setting table

Combination number	***n***	***d*** **(mm)**	**combination number**	***n***	***d*** **(mm)**	**Combination number**	***n***	***d*** **(mm)**
1	1	1	11	1.4	1	21	1.8	1
2	1	2	12	1.4	2	22	1.8	2
3	1	3	13	1.4	3	23	1.8	3
4	1	4	14	1.4	4	24	1.8	4
5	1	5	15	1.4	5	25	1.8	5
6	1.2	1	16	1.6	1	26	2	1
7	1.2	2	17	1.6	2	27	2	2
8	1.2	3	18	1.6	3	28	2	3
9	1.2	4	19	1.6	4	29	2	4
10	1.2	5	20	1.6	5	30	2	5

Note: n= Talbot exponent; d= outlet aperture (mm).

According to the capacity of the device and referring to the previous results [7] [27], the total mass of the sample is controlled to be 160 g, the filling height is 5.7 cm, and the initial porosity is about 0.41. The inlet water pressure is 0.5 MPa, and the outlet end is connected to the atmosphere. In addition to the broken mudstone particles, the test also uses aeolian sand as the source of external migration particles to simulate the process of loose overburden particles entering the broken rock mass and participating in the migration under the hydraulic action. The sand source is Maowusu desert aeolian sand with a particle size of 0.074-0.65 mm. The mass of each test sand source is 45 g. Under the premise of keeping the type of particle material and other conditions unchanged, only the particle gradation or outlet scale is changed, so as to ensure that different test combinations have consistent initial structure and seepage conditions, and it is convenient to compare their seepage response and particle migration differences.

153 **2.2.3 Test procedure**

154 The process of seepage and sand burst test of broken rock mass is shown in fig. 5. The test mainly includes system
155 commissioning, sample loading, sand source layout, permeable plate installation, constant pressure seepage test and post-
156 test treatment.

157 (1) System commissioning. Before the formal test, the pressure supply system, seepage test apparatus and data
158 acquisition system are connected to check the sealing of each pipeline and connection part, and the pressure sensor and
159 flow sensor are checked to ensure the stable working state of the system.

160 (2) Install and test the cylinder (Fig.5a). After the system commissioning is completed, the internal and thread
161 connection parts of the cylinder are cleaned first to prevent the residual particles from affecting the assembly tightness.
162 Subsequently, the upper and lower pistons and compression devices are installed, and the pressure performance is tested
163 to be stable.

164 (3) Permeable plate installation (Fig. 5b). According to the test grouping, the corresponding aperture permeable plate
165 is selected and installed at the outlet end to ensure that the permeable plate is firmly connected with the permeameter
166 cylinder to avoid particle flow or side leakage.

167 (4) Sample filling (Fig. 5c). According to the particle gradation shown in Table 1, the mudstone particles with different
168 particle sizes were weighed, fully mixed and loaded into the permeameter cylinder. By controlling the total mass and
169 filling height of the sample, the sample reached the target porosity condition. In the filling process, the particle distribution
170 should be ensured as much as possible to avoid local segregation.

171 (5) Sand source arrangement (Fig.5d). A 45 g aeolian sand source was added to the upstream sand storage tank of the
172 sample, so that the sand source could enter the broken rock mass under the action of constant water pressure during the
173 test, and the process of the overlying loose layer particles participating in the seepage-induced sand inrush was simulated.

174 (6) Constant pressure seepage loading and monitoring (Fig.5e). The pressure-supply system was activated and ... was
175 maintained... the inlet water pressure at 0.5 MPa. During the test, the pressure and flow data were recorded in real time,
176 and the outflow particles were continuously collected. The phenomena of particle flow, local clogging and continuous
177 sand inrush under different test combinations were observed.

178 (7) Post-processing (Fig 5f). After the test, the pressure supply system was closed, the seepage test apparatus was
179 disassembled, and the outflow particles were dried and weighed. The samples after the test were screened to analyze the
180 loss characteristics of different particle size components and the change of gradation after the test.



(a) Install and test the cylinder



(b) Installation of permeable plate



(c) Filling of broken rock mass



(d) Filling of sand source



(e) Constant pressure seepage loading



(f) The collected sand particles are weighed after drying.

Fig.5 Experimental procedure

2.2.4 Evaluation indices and calculation methods for seepage-induced sand inrush

(1) Equivalent permeability

During each test, outlet flow rate was recorded continuously under constant inlet water pressure the inlet water pressure was kept constant, and the average flow rate in the stable seepage stage was selected to calculate the equivalent permeability. According to Darcy 's law [28-29], the equivalent permeability can be expressed as:

$$k = -\frac{\mu Q \mathrm{d}z}{A \mathrm{d}P} = \frac{\mu Q h}{A P} \tag{3}$$

In the formula: k is the equivalent permeability, m^2; μ is hydrodynamic viscosity, Pa · s; q is the average flow rate in the steady seepage stage, m^3/s ; h is the height of broken rock mass sample, m; A is the cross-sectional area of the infiltration tube, m^2; ΔP is the pressure difference between the two ends of the sample, Pa.

Because the particle migration, deposition and loss during the test will cause the dynamic change of the pore structure inside the sample, the system is not a stable homogeneous porous medium in the strict sense. Therefore, in this paper, the permeability parameters calculated based on the macroscopic flow rate and pressure difference in the steady seepage stage are defined as ' equivalent permeability ', which is mainly used to compare the relative difference of the overall conductivity of the particle system under different test combinations.

Taking n = 1.6, $F_f = 2.00\%$, d = 3 mm test combination (No.18) as an example, the average flow rate in the stable seepage stage is 125.92 mL / min, which is converted into:

$$\bar{Q} = \frac{125.92 \times 10^{-6}}{60} = 2.0987 \times 10^{-6}\ \mathrm{m^3/s}.$$

The dynamic viscosity of water was set as $\mu = 1.0 \times 10^{-3}$ Pa · s, the specimen height was L = 0.057 m, the cross-sectional area of the permeameter was $A = 4.6633 \times 10^{-4}$ m², and the pressure difference across the specimen was ΔP = 0.5 MPa = 5.0×10^5 Pa. Therefore, the equivalent permeability of this test condition was calculated as follows:

$$k = \frac{\mu \bar{Q} L}{A \Delta P} = \frac{1.0 \times 10^{-3} \times 2.0987 \times 10^{-6} \times 0.057}{4.6633 \times 10^{-4} \times 5.0 \times 10^5} = 5.1304 \times 10^{-13}\ \mathrm{m^2}.$$

(2) Total sand discharge

In this paper, the cumulative mass of particles discharged from the outlet during the whole process of a single set of tests is defined as the total sand discharge. During the test, the particles discharged from the outlet were continuously collected. After the test, the particles were uniformly dried and weighed to obtain the total sand discharge under the

corresponding test combination.

Since both the externally supplied aeolian sand and the fine particles migrating from the broken mudstone may participate in the particle transport process during the tests, and the two sources are difficult to distinguish completely during outlet collection, all discharged particles are uniformly defined as the cumulative sand discharge during seepage-induced sand inrush. This parameter is used to characterize the degree of particle release under different particle gradations and outlet conditions, without further distinguishing the particle sources. The cumulative sand discharge can be expressed as:

$$M_S = \Sigma \Delta m \tag{4}$$

In the formula: M_s represents the cumulative sand discharge mass (g), and Δm represents the mass of particles discharged during each time interval (g).

Taking the test condition with $n = 1.6$, $F_f = 2.00\%$, and $d = 3$mm (No. 18) as an example, the oven-dried masses of discharged particles collected during each interval throughout the entire test process were accumulated to obtain:

$$M_s = \sum_{i=1}^{N} m_i = 3.52 + 1.03 + 0.57 = 5.12 \text{ g}$$

(3) Time to first sand emergence

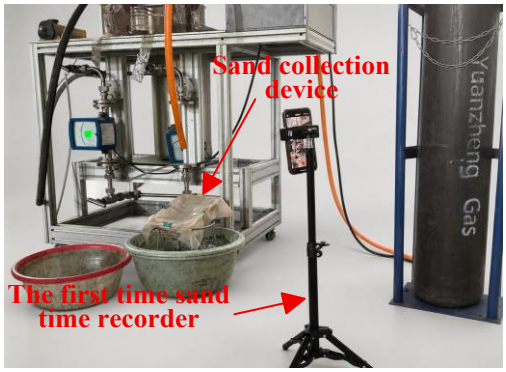


Fig. 6 First sand time recording device

In this paper, the device shown in Fig. 6 was used to define the time elapsed from the moment when the inlet water pressure was applied to the moment when identifiable particles were first observed to be discharged with the water flow at the specimen outlet as the time to first sand emergence, denoted as t_s. The time to first sand emergence (t_s) represents the outlet response time after the initiation of particle migration rather than the critical hydraulic gradient in the strict sense. Its expression is given as follows:

$$t_s = t_1 - t_0 \tag{5}$$

In the formula: t_s represents the time to first sand emergence (s); t_0 represents the moment when the water pressure was applied and timing was initiated (s); and t_1 represents the moment when identifiable particles were first observed to be discharged with the water flow at the specimen outlet (s).

During the experiments, the moment of first sand emergence was determined jointly through visual observation and

video recording. When only clear water flowed out from the specimen outlet without obvious particle discharge, timing was continued. When identifiable particles were first observed to be discharged with the water flow at the outlet, this moment was recorded as the time to first sand emergence. To reduce errors caused by manual identification, each test condition was repeated three times, and the average value of the three measurements was taken as the time to first sand emergence for that test condition.

3. Results and analysis

The equivalent permeability (k), total sand discharge (M_s), time to first sand emergence (t_s), and seepage-induced sand inrush phenomena of broken rock masses under different test conditions are summarized in Table 3. As shown in the table, significant differences exist in the seepage-induced sand inrush evaluation indicators and experimental phenomena among different combinations of Talbot gradation and permeable-plate aperture. Based on these observations, the variations in each evaluation indicator of seepage-induced sand inrush are first analyzed. Subsequently, the seepage-induced sand inrush response modes are classified according to the macroscopic experimental phenomena, and the distribution characteristics of different modes under various gradation–outlet aperture combinations are further investigated.

Table 3. Experimental results of seepage-induced sand inrush in broken rock masses under the coupled effects of particle gradation and outlet aperture

combination number	***n***	***d*** **(mm)**	***K*** **($10^{-13}m^2$)**	***Ms*** **(g)**	***ts*** **(s)**	**Observed phenomena**
1	1	1	1.98	0.5	15	Significant clogging occurred during the initial stage, resulting in no water discharge for a relatively long period. Subsequently, only a small amount of fine mudstone particles was discharged, with no obvious sand particle release observed.
2	1	2	2.88	1.35	4	The initial clogging duration was relatively long, and water discharge was significantly delayed. Particle output was dominated by fine mudstone particles, with insignificant sand release.
3	1	3	3.17	1.68	3	Water discharge began after a short delay and was accompanied by the slow discharge of a small amount of sand particles.
4	1	4	3.69	1.96	3	After water discharge began, a small amount of sand-particle release was observed; the overall sand-discharge intensity remained low.

5	1	5	4.09	4.98	2	Particles were discharged slowly and continuously at low intensity.
6	1.2	1	2.36	1.48	13	Water discharge developed slowly, followed by the slow and continuous release of a small amount of sand particles.
7	1.2	2	3.52	1.63	3	Particle output was low and mainly consisted of fine mudstone particles, with only a very small amount of sand particles.
8	1.2	3	3.68	1.96	2	The seepage velocity was relatively low, accompanied by slow release of a small amount of sand particles.
9	1.2	4	3.90	2.23	3	The initial seepage rate was low, followed by the gradual release of a small amount of sand particles.
10	1.2	5	5.53	5.32	2	The initial flow velocity was low, followed by an obvious increase in flow velocity and subsequent transition to slow continuous sand discharge.
11	1.4	1	2.69	1.69	8	Sudden particle release caused pronounced concentrated sand inrush over a short period.
12	1.4	2	4.00	2.38	3	Sudden particle release occurred, accompanied by rapid concentrated particle discharge and evident sand-inrush characteristics.
13	1.4	3	4.06	2.95	2	The overall seepage process was relatively slow, and sand particles were continuously released with water flow.
14	1.4	4	4.10	3.65	2	Particle-output intensity was low and was dominated by fine mudstone particles, with only a very small amount of sand particles.
15	1.4	5	7.14	9.8	1	The seepage process was relatively slow, with only a small amount of sand particles released continuously.
16	1.6	1	2.81	2.01	6	Water discharge was slow initially, followed by the gradual slow release of sand particles.
17	1.6	2	4.62	4.96	3	Sudden concentrated sand inrush occurred, with particles discharged rapidly over a short period.
18	1.6	3	5.13	5.12	2	Sudden concentrated sand inrush occurred, with a relatively high particle-release intensity.
19	1.6	4	5.53	5.35	2	Particle output remained low and consisted mainly of fine mudstone particles, with only a small amount of sand particles.

20	1.6	5	7.75	22	1	A small amount of sand particles was released after water discharge began, showing overall weak but sustained sand discharge.
21	1.8	1	2.84	2.33	5	The initial seepage process was slow, followed by a gradual transition to slow sustained sand discharge.
22	1.8	2	6.22	18.5	1	The initial flow was slow, followed by pronounced sustained particle release.
23	1.8	3	6.54	19.64	1	Sudden concentrated sand inrush occurred, with rapid and large-scale particle discharge.
24	1.8	4	7.59	20.94	1	Sudden concentrated sand inrush occurred, accompanied by strong sustained particle output.
25	1.8	5	8.00	23.8	1	The initial seepage process was slow, followed by sustained slow sand discharge.
26	2	1	2.90	2.55	5	The initial flow was slow, followed by the gradual onset of slow sustained sand discharge..
27	2	2	6.37	19.8	1	A short-duration sudden sand inrush occurred; concentrated particle release was brief and then weakened markedly.
28	2	3	7.15	21.34	1	Sudden concentrated sand inrush occurred, accompanied by rapid, large-volume particle discharge.
29	2	4	7.73	23.85	1	Sudden concentrated sand inrush occurred, with rapid particle discharge and strong persistence.
30	2	5	8.18	26.8	1	Sudden concentrated sand inrush occurred, with rapid, large-volume particle discharge and clear sustained sand-discharge characteristics.

Note: n= Talbot exponent; d= outlet aperture (mm); K= equivalent permeability (m²); M_s= total sand discharge (g); t_s= time to first sand emergence (s).

3.1 Seepage-induced sand-inrush characteristics

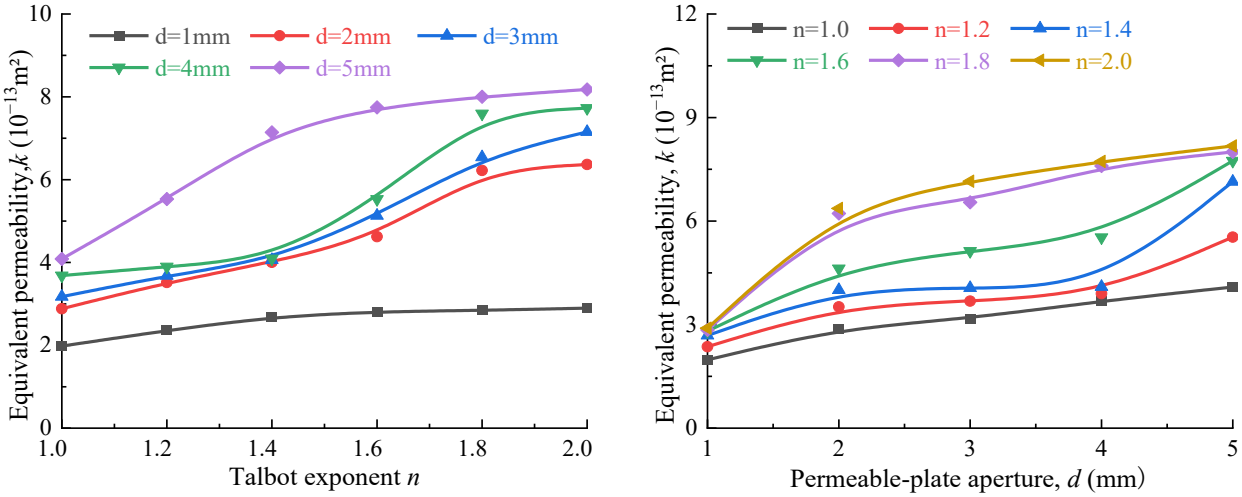
3.1.1 Equivalent permeability

According to the experimental results in Table 3, the variation curves of the equivalent permeability of broken rock masses under different Talbot gradations and permeable-plate apertures are shown in Fig. 7. With increasing Talbot exponent $n$from 1.0 to 2.0, the mass fraction of mudstone particles smaller than 0.8 mm decreases from 8.00% to 0.60%, and the equivalent permeability increases by 46.3%–125.4% for different aperture groups (Fig. 7(a)). Under relatively low $n$conditions, the fine mudstone particles exhibit a strong filling effect on the pores within the coarse-particle skeleton and are prone to forming local bridging structures near the permeable plate, thereby restricting effective seepage channels and

resulting in relatively low equivalent permeability. With increasing n, the content of fine particles decreases, weakening the particle-filling effect. Consequently, the effective flow space and pore connectivity inside the specimen are improved, leading to an increase in equivalent permeability at the macroscopic scale. In particular, when $n$increases from 1.6 to 1.8, the equivalent permeability of the 2, 3, and 4 mm aperture groups increases by 34.5%, 27.5%, and 37.4%, respectively, indicating that the connectivity of effective seepage channels is significantly enhanced within this gradation range. In contrast, the 1 mm aperture group is strongly affected by outlet geometric constraints. When $n$further increases from 1.8 to 2.0, the equivalent permeability only increases from 2.84×10^{-13}m² to 2.90×10^{-13}m², with an increase of less than 2%. This indicates that strong outlet geometric constraints weaken the enhancement effect of improved internal pore structures on the macroscopic flow capacity.

Regarding the effect of permeable-plate aperture, when the aperture increases from 1 mm to 5 mm, the equivalent permeability of all Talbot gradation groups increases by 106.4%–182.3% (Fig. 7(b)). Under the conditions of $n = 1.8$and $n = 2.0$with relatively low fine-particle contents, increasing the aperture from 1 mm to 2 mm increases the equivalent permeability by 118.8% and 119.8%, respectively. This indicates that the particle-filling effect is relatively weak under these conditions, and even a slight increase in outlet aperture can significantly reduce particle sieving and bridging constraints, thereby rapidly improving the connectivity of restricted seepage channels. With increasing content of mudstone fine particles, the sensitive range of equivalent permeability to outlet aperture gradually shifts toward larger apertures. For the $n = 1.4$and $n = 1.6$groups, significant increases mainly occur within the 4–5 mm aperture range. For the $n = 1.0$group, although the equivalent permeability increases from 1.98×10^{-13}m² to 4.09×10^{-13}m² when the permeable-plate aperture increases from 1 mm to 5 mm, the increase between subsequent adjacent aperture intervals is relatively limited. This indicates that a higher content of fine particles increases the initial pore-filling degree, thereby weakening the enhancement effect of increasing outlet aperture on the overall flow capacity.

Overall, the equivalent permeability of broken rock masses exhibits an overall nonlinear increasing trend with increasing Talbot exponent and permeable-plate aperture. However, the increasing magnitude and sensitive ranges vary significantly under different combinations. Under conditions of low Talbot exponent or small aperture, the equivalent permeability remains relatively low. With further increases in gradation parameters and outlet aperture, some combinations enter a stage of pronounced permeability increase, showing evident stage-dependent characteristics and differences among different parameter combinations.



(a) Effect of different Talbot exponents

(b) Effect of different outlet apertures

Fig. 7. Variation of equivalent permeability under different Talbot exponents and permeable-plate apertures

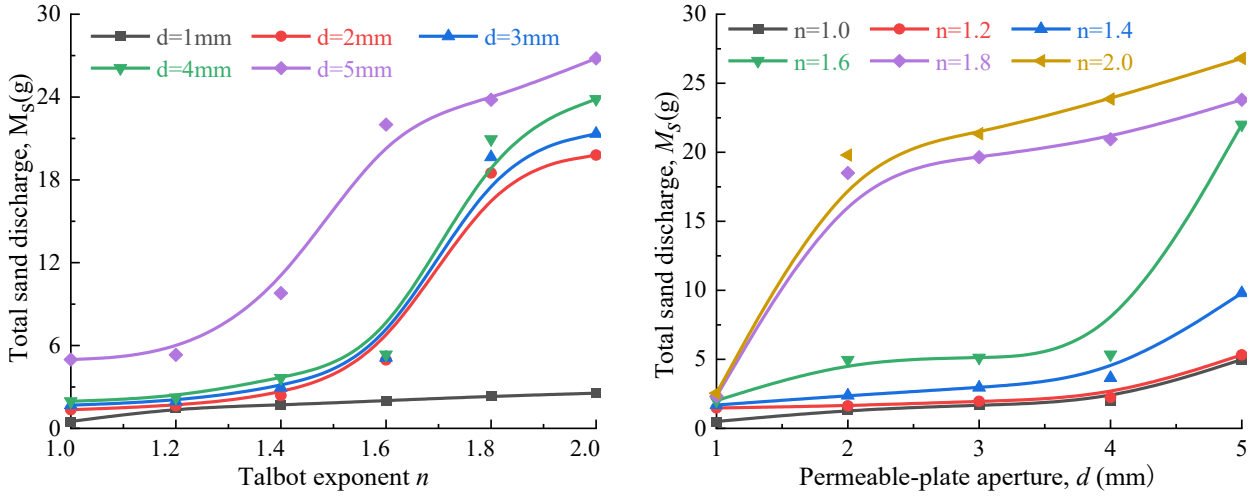
3.1.2 Total sand discharge

According to the experimental results in Table 3, the variation curves of total sand discharge of broken rock masses under different Talbot gradations and permeable-plate apertures are shown in Fig. 8. With increasing Talbot exponent n from 1.0 to 2.0, the total sand discharge increases by 410.0%–1366.7% under different permeable-plate aperture conditions (Fig. 8(a)). Under relatively low n conditions, the content of mudstone fine particles in the specimen is relatively high. Migrating particles are prone to accumulate within the pores of the coarse-particle skeleton and near the permeable plate, and particle migration is mainly characterized by local retention and slow release. With increasing n, the content of mudstone fine particles decreases, weakening the filling and bridging effects. Consequently, particles can more easily overcome local constraints under hydraulic action and migrate toward the outlet. In particular, when n increases from 1.6 to 1.8, the total sand discharge of the 2–4 mm aperture groups rapidly increases from approximately 5 g to 18.50–20.94 g, corresponding to an increase of 273.0%–291.4%. This indicates that particle migration within this gradation range rapidly transforms from a locally constrained state to concentrated release.

Regarding the effect of outlet aperture, the Talbot gradation range corresponding to significant increases in total sand discharge gradually shifts toward lower n values with increasing outlet aperture (Fig. 8(b)). Under the 5 mm aperture condition, when n increases from 1.2 to 1.4, the total sand discharge increases from 5.32 g to 9.80 g. With a further increase to $n = 1.6$, the total sand discharge reaches 22.00 g, representing an increase of 124.5% within this stage. In contrast, although the total sand discharge of the 1 mm aperture group increases from 0.50 g to 2.55 g with increasing Talbot exponent, it remains at a relatively low level overall. When the permeable-plate aperture increases from 1 mm to 5 mm, the total sand discharge of different gradation groups increases by 259.5%-994.5%. For $n = 1.8$ and $n = 2.0$, increasing the aperture from 1 mm to 2 mm increases the total sand discharge from 2.33 g and 2.55 g to 18.50 g and 19.80 g, respectively, corresponding to increases of 694.0% and 676.5%. For $n = 1.4$ and $n = 1.6$, significant increases mainly occur at larger apertures. When the aperture increases from 4 mm to 5 mm, the total sand discharge increases from 3.65 g and 5.35 g to 9.80 g and 22.00 g, respectively, with the $n = 1.6$ group showing an increase of 311.2%. For the $n = 1.0$ and

$n = 1.2$groups, the total sand discharge remains below 3 g within the aperture range of 1-4 mm.

In summary, the total sand discharge of broken rock masses increased markedly and nonlinearly with increasing Talbot exponent and permeable-plate aperture. The variation magnitude is considerably larger than that of equivalent permeability, indicating that the particle release process is more sensitive to changes in particle gradation and outlet boundary conditions. Under different parameter combinations, the total sand discharge shows significant differences: low Talbot exponent combined with small aperture conditions maintains a relatively low particle discharge level, whereas high Talbot exponent combined with large aperture conditions results in significantly increased particle outflow.



(a) Effect of different Talbot exponents

(b) Effect of different outlet apertures

Fig. 8. Variation of total sand discharge under different Talbot exponents and permeable-plate apertures

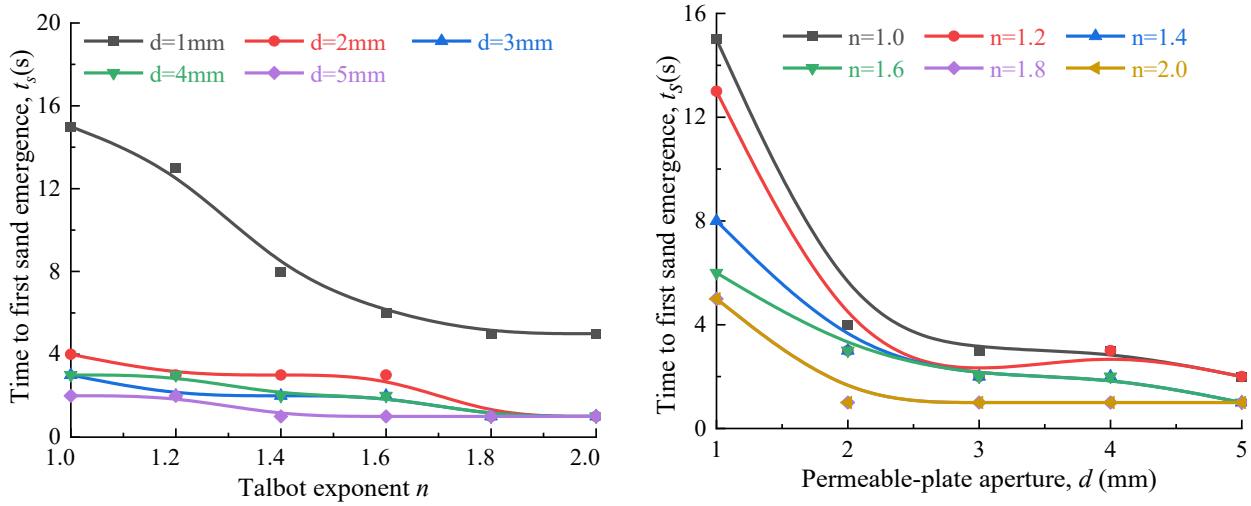
3.1.3 Time to first sand emergence

According to the experimental results in Table 3, the variation curves of the time to first sand emergence of broken rock masses under different Talbot gradations and permeable-plate apertures are shown in Fig. 9. With increasing Talbot exponent n, the content of mudstone fine particles gradually decreases, weakening the filling effect of particles within the pores of the coarse-particle skeleton and the bridging effect near the outlet. Consequently, migrating particles can more easily overcome local constraints and reach the outlet. For the 1 mm aperture group, the time to first sand emergence decreases from 15 s to 5 s, representing a reduction of 66.7%. For the 2–4 mm aperture groups, the time to first sand emergence mainly remains within 2–4 s under low and intermediate $n$conditions, but decreases to approximately 1 s when $n$increases to 1.8. This indicates that the reduction in mudstone fine-particle content enables particles to overcome the original local constraints more rapidly (Fig. 9(a)). For the 5 mm aperture group, the time to first sand emergence remains within 1–2 s overall and approaches 1 s under higher Talbot exponent conditions, indicating that particle initial discharge occurs earlier under larger outlet aperture conditions.

Regarding the effect of outlet aperture, when the permeable-plate aperture increases from 1 mm to 5 mm, the time to first sand emergence decreases by 80.0%-87.5% for all Talbot gradation groups. Specifically, for the $n = 1.0$group, the time decreases from 15 s to 2 s; for the $n = 1.4$group, it decreases from 8 s to 1 s; and for the $n = 1.8$and $n = 2.0$groups, it decreases from 5 s to 1 s (Fig. 9(b)). Under small aperture conditions, particles experience stronger sieving and bridging

constraints when passing through the outlet, requiring a certain period of migration and local adjustment before discharge. With increasing outlet aperture, these restrictions gradually weaken, resulting in a significant reduction in the time to first sand emergence. When the aperture reaches 4-5 mm, the time to first sand emergence for all gradation groups gradually approaches 1-2 s, indicating that the limiting effect of outlet aperture on the initial particle discharge is significantly weakened when the aperture reaches 4-5 mm.

In summary, the time to first sand emergence of broken rock masses decreased as the Talbot exponent and permeable-plate aperture increased, indicating that particle gradation and outlet aperture jointly influence the initial outlet response of particles. Compared with equivalent permeability and total sand discharge, the time to first sand emergence more directly reflects the early response characteristics of particles reaching the outlet.



(a) Effect of different Talbot exponents (b) Effect of different outlet apertures

Fig. 9. Variation of time to first sand emergence under different Talbot exponents and permeable-plate apertures

3.2 Seepage-induced sand-inrush modes

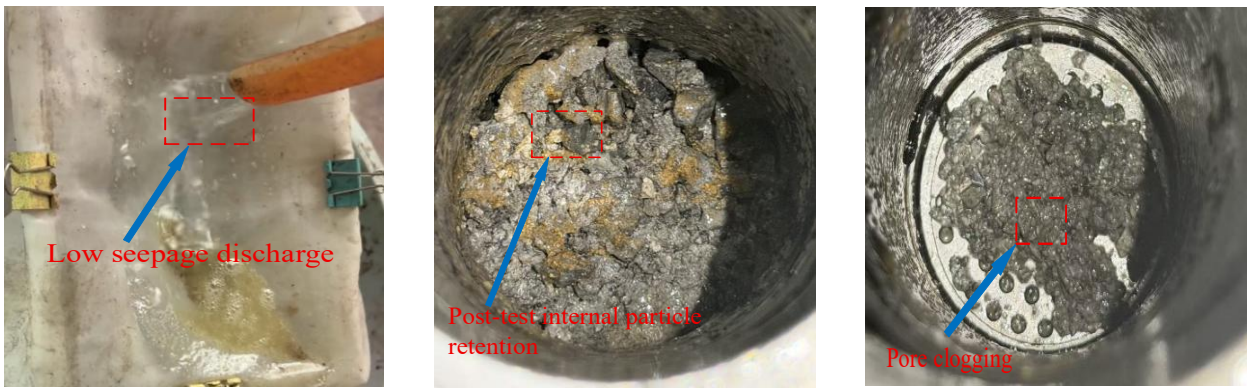
Based on the seepage-induced sand inrush phenomena and evaluation indicators of each test condition in Table 3, the seepage-induced sand inrush behavior of broken rock masses was classified into three modes: Type I: migration-deposition-clogging-slow-release mode, Type II: local clogging-staged release mode, and Type III: channel breakthrough-sustained discharge mode.

(1) Type I: Migration-deposition-clogging-slow-release mode

As shown in Table 3, this mode mainly occurs under the combination conditions of relatively low Talbot exponent and small permeable-plate aperture. The corresponding test conditions mainly include most groups within the ranges of $n = 1.0$-1.6 and $d = 1$-3 mm (Test conditions: 1-4, 6-9, 11-13, 16, 21, and 26). During the tests, a small amount of particles was observed to migrate with the water flow at the outlet. Subsequently, some particles deposited near the permeable plate, and the particle release intensity gradually decreased, exhibiting an evident slow-release characteristic (Fig. 10(a)). After the completion of the tests, the coarse-particle skeleton inside the sleeve remained relatively intact, with a large number of par

ticles retained within the specimen and local accumulation of fine particles observed (Fig. 10(b)). With co ntinuous accumulation of migrating particles, a particle covering layer gradually formed on the surface of the permeable plate. Some apertures were restricted by deposited particles, resulting in a certain degree of clogging near the outlet region (Fig. 10(c)).

To further characterize this sand-inrush behavior, the equivalent permeability, total sand discharge, an d time to first sand emergence of the specimens were analyzed. The results show that most test conditio ns satisfy $k \leq 4.10 \times 10^{-13}\text{m}^2$, $M_s \leq 3.0\text{g}$, and $t_s \geq 3\text{s}$. Although some individual test conditions exhibite d short-term local breakthrough during the tests, they were still classified as Type I when the overall equ ivalent permeability and total sand discharge remained within a low range and no sustained large-scale sa nd discharge occurred after the breakthrough. This classification avoids misjudgment caused solely by tran sient particle discharge phenomena. This mode is characterized by weaker outlet release capacity than fine -particle clogging capacity, resulting in low particle discharge and weak seepage response.



(a) Weak particle discharge at outlet

(b) Post-test internal particle retention

(c) Particle retention and local fine accumulation

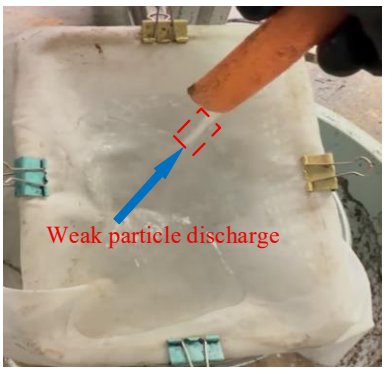
Fig. 10. Typical experimental phenomena of the Type I migration-deposition-clogging-slow-release mode

(2) Type II: Local clogging-staged release mode

As shown in Table 3, this mode is mainly distributed under transitional conditions with moderate Talbot e xponents and permeable-plate apertures. The corresponding test conditions mainly include some groups within t he ranges of $n = 1.4\text{-}1.8$ and $d = 3\text{-}5$ mm (Test conditions: 5, 10, 14, and 17-19). During the tests, particle re lease at the outlet under Type II conditions exhibited a pronounced staged characteristic. Before concentrated r elease, only a small amount of particles was discharged with the water flow, and the overall sand-inrush inten sity remained relatively low (Fig. 11(a)). Subsequently, the particle discharge increased rapidly within a short p eriod, resulting in local concentrated release (Fig. 11(b)). After the concentrated release stage, the particle disch arge intensity at the outlet decreased again (Fig. 11(c)).

Post-test observations showed that fine particles mainly filled the spaces between coarse particles and form ed local accumulations, while a certain amount of effective flow space remained inside the specimen (Fig. 11

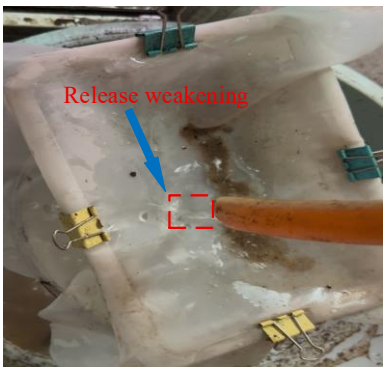
(d)). Only some apertures on the surface of the permeable plate remained open, whereas the other apertures exhibited different degrees of particle deposition and coverage, indicating the formation of a localized clogging zone near the outlet (Fig. 11(e)). Based on this sand-inrush behavior, the equivalent permeability, total sand discharge, and time to first sand emergence were further analyzed. The results show that these test conditions generally exhibit an intermediate response level, mainly satisfying: $k = 4.09\text{-}5.53 \times 10^{-13}$ m^2, $Ms = 3.65\text{-}5.35$ g, $t_s = 2\text{-}3$ s. Fig 11(a)-(c) show outlet images of the same test condition at consecutive time intervals. The classification of Type II should simultaneously satisfy two criteria: the evaluation indicators fall within the intermediate response range, and the discharge process exhibits an evident staged characteristic. Therefore, Type II should not simply be regarded as the remaining test conditions after excluding Type I and Type III modes. This mode reflects the dynamic competition between local particle clogging and outlet particle release. Local clogging can form but has limited stability; under continuous hydraulic action, it may undergo local instability and induce staged particle release. Therefore, this mode represents a transitional state during the evolution from stable clogging to continuous channel connectivity.



(a) Pre-release stage with weak particle discharge



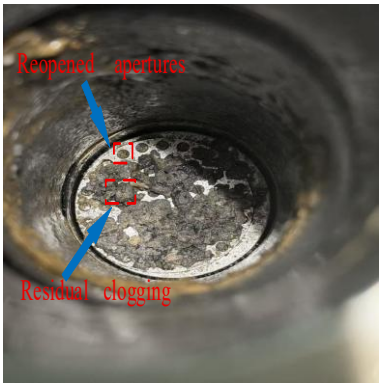
(b) Concentrated particle release following local breakthrough



(c) Weakened particle release after breakthrough



(d) Local particle loss after the test



(e) Partial aperture reopening with residual particle clogging

Fig. 11. Time-sequential experimental phenomena of staged concentrated release in a typical test conditio

(3) Type III: Channel breakthrough–sustained discharge mode

As shown in Table 3, this mode is mainly distributed under the combination conditions of relatively high Talbot

exponent and large permeable-plate aperture. The corresponding test conditions mainly include the ranges of $n = 1.8$–2.0 and $d = 2$–5 mm, as well as some transitional conditions with large apertures (Test conditions: 15, 20, 22–25, and 27–30). During the tests, after water pressure loading, particles rapidly migrated toward the outlet. A preferential sand discharge channel gradually developed near the outlet, followed by continuous particle discharge with the water flow, exhibiting an evident sustained discharge characteristic.

Throughout the entire testing process, the particle discharge intensity remained relatively high, and a large amount of discharged particles accumulated in the outlet region. The total sand discharge was significantly higher than those of the previous two modes (Fig. 12(a)). After the completion of the test, the particle distribution inside the sleeve exhibited significant spatial heterogeneity. Obvious particle loss occurred in local regions, the integrity of the original particle skeleton was reduced, and a highly continuous seepage channel was formed (Fig. 12(b)). Most apertures on the surface of the permeable plate remained exposed or reopened, with only a small amount of coarse particles and residual particles covering the outlet surface. This indicates that a stable deposition-clogging structure was difficult to maintain near the outlet, and the particle release process gradually became dominant (Fig. 12(c)).

Based on this sand-inrush behavior, the equivalent permeability, total sand discharge, and time to first sand emergence were further analyzed. The results show that most test conditions satisfy: $k \geq 6.0 \times 10^{-13}$ m^2, $M_s \geq 9.0$ g, $t_s \leq 1$. This mode is characterized by a high particle release intensity and the rapid development of dominant seepage channels.



(a)Pronounced particle deposition after sustained discharge

(b)Internal structural loosening and heterogeneous particle loss

(c)Extensive aperture exposure with weak residual clogging

Fig. 12. Typical experimental phenomena of the channel breakthrough–sustained discharge mode

Based on the above mode classification and analysis of typical characteristics, the 30 test conditions were categorized and statistically analyzed. The numbers of Type I, Type II, and Type III test conditions were 14, 6, and 10, respectively, as shown in Fig. 13. The three seepage-induced sand inrush modes exhibit distinct zonal characteristics within the Talbot gradation–permeable-plate aperture combination space. Among them, the Type I mode is mainly concentrated in the region with a high content of mudstone fine particles or small permeable-plate apertures. Under these test conditions, the system exhibits characteristics of local clogging and slow sand discharge. The Type III mode mainly occurs in regions with a low content of fine particles and large permeable-plate apertures. Under these conditions, particle migration is relatively sufficient, exhibiting rapid channel breakthrough and sustained particle discharge characteristics. The Type II mode is mainly distributed in the transition region between Type I and Type III modes, exhibiting staged release

characteristics.These results indicate that the modes were not randomly distributed but formed systematic zones during the coupled variation of gradation parameters and outlet aperture. Compared with the control of a single factor, the outlet aperture changes the critical transition range between different modes under various gradation conditions, while particle gradation determines the sensitivity of the system to variations in outlet aperture. Therefore, particle gradation and outlet aperture exhibit significant coupled regulation characteristics in controlling the evolution of seepage-induced sand inrush modes.

Further analysis shows that, when the permeable-plate aperture remains constant, the mode distribution gradually shifts from the Type I region toward the Type II and Type III regions with a gradual decrease in the mass fraction of fine particles. This indicates that different gradation conditions lead to distinct sand-inrush response modes. Under a constant particle gradation condition, increasing the permeable-plate aperture also causes the mode distribution to transition from Type I toward Type II and Type III. Larger apertures are therefore more likely to induce Type II and Type III responses.

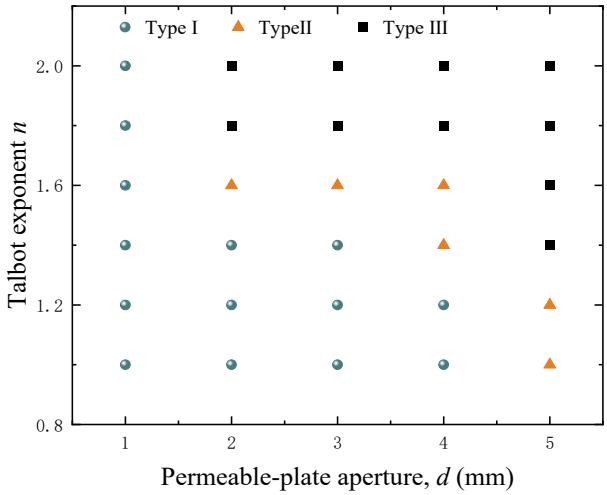


Fig. 13. Distribution of seepage-induced sand inrush response modes under different particle gradations and permeable-plate apertures

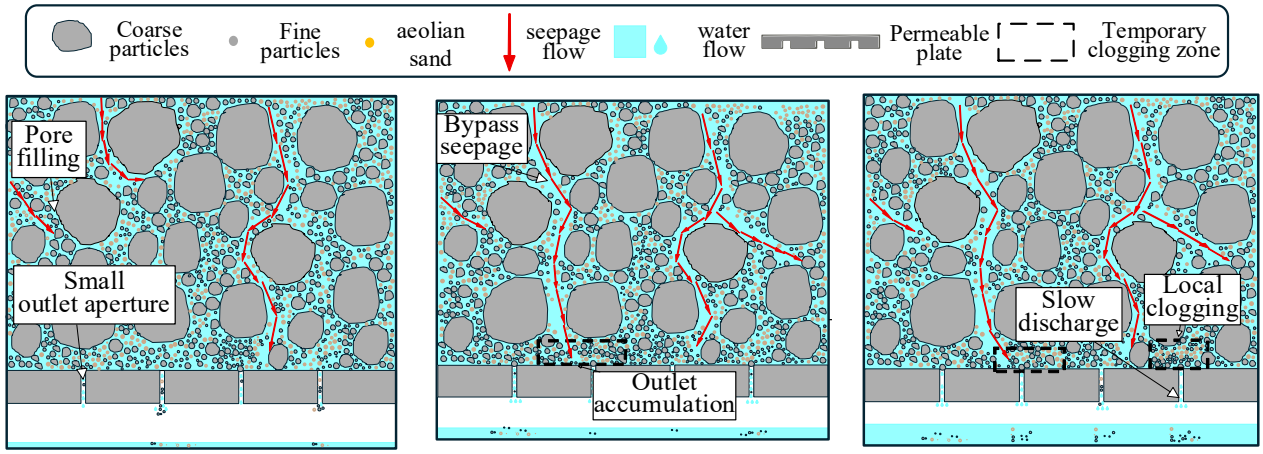
4. Evolution mechanisms of seepage-induced sand inrush in broken rock masses under different particle gradations and outlet boundary conditions

4.1 Evolution mechanism of Type I: migration–deposition–clogging–slow-release mode

When the local filling–clogging capacity is significantly higher than the outlet release capacity, the broken rock mass exhibits the migration–deposition–clogging–slow-release mode (Type I) of seepage-induced sand inrush (Fig. 14). Under this condition, the relatively high content of mudstone fine particles enables them to sufficiently fill the pores within the coarse-particle skeleton, thereby reducing the effective flow space and resulting in a relatively high degree of pore filling within the particle system (Fig. 14(a)). During seepage, both the mudstone fine particles and the sand-source particles entering the specimen may migrate and become retained and deposited near the outlet under geometric constraints (Fig. 14(b)). With continuous accumulation of deposited particles, some apertures are initially covered. Subsequently, the deposited particles interlock with the surrounding coarse particles and gradually form a local filling–bridging structure. This further increases the local seepage resistance near the outlet, causing subsequent migrating particles to be

continuously retained on its upstream side and gradually forming a relatively stable local clogging zone (Fig. 14(c)). During this process, the supply of particles to the clogging zone and the formation of the clogging structure are generally faster than the process of hydraulic destruction and release. Therefore, the local clogging can remain relatively stable. After local clogging is formed, the further expansion of the dominant seepage channels is restricted, which is macroscopically reflected by relatively low equivalent permeability, low total sand discharge, and a relatively delayed time to first sand emergence.

Overall, the evolution pathway of Type I mode can be described as: pore filling → fine-particle migration → outlet deposition → filling–bridging → stable localized clogging → bypass seepage. The essence of this sand-inrush mode is that fine particles do not cease migrating; instead, the migrating particles near the outlet gradually transform into an important component of the clogging structure, thereby continuously restricting subsequent particle release and the expansion of dominant seepage channels.



(a) Pore filling under high fine-particle content

(b) Fine migration and outlet accumulation

(c) Local clogging under strong outlet constraint

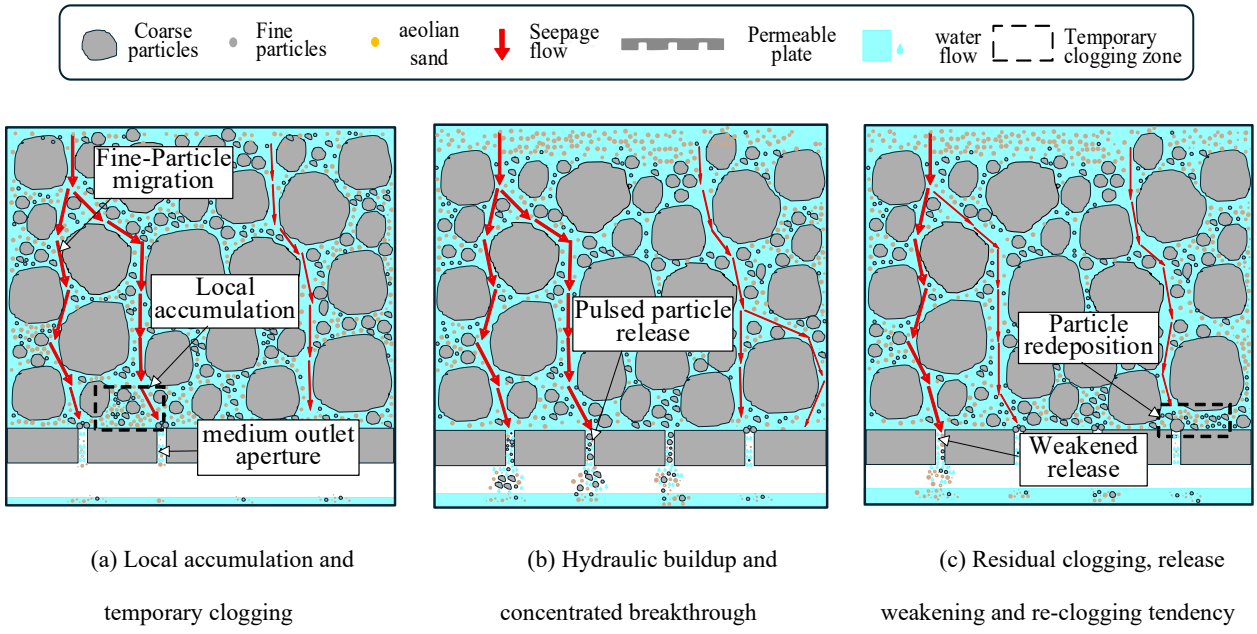
Fig. 14. Formation mechanism of the Type I migration–deposition–clogging–slow-release mode

4.2 Cyclic evolution mechanism of Type II: local clogging–staged release mode

When the local particle clogging effect and outlet release capacity are comparable, the broken rock mass exhibits the local clogging–staged release mode (Type II) of seepage-induced sand inrush (Fig. 15). Under this condition, fine particles can still deposit within the pores of the particle skeleton and near the permeable plate; however, the formed clogging structure is relatively weak in terms of thickness, continuity, and interlocking degree between particles, and therefore remains in a metastable state. After temporary clogging forms, the effective flow area near the outlet decreases, and the obstruction effect of the clogging region on water flow is enhanced, causing seepage flow to gradually concentrate toward weak zones within the clogging structure (Fig. 15(a)).When the drag force of water flow and local pressure exceed the stable bearing capacity of the clogging structure, the clogging body first undergoes local instability at structurally weak regions. Subsequently, the previously restricted water flow and particles rapidly concentrate toward the breakthrough location, resulting in a significant increase in the particle release rate within this region over a short period (Fig. 15(b)). After local breakthrough occurs, the previously restricted water flow upstream of the clogging body is rapidly released.

The concentration effect of water flow within the breakthrough region gradually weakens, and the drag force acting on particles correspondingly decreases. Meanwhile, some deposited particles that have not been washed away remain on the surface of the permeable plate, and migrating particles inside the specimen continue to be supplied toward the outlet. Therefore, particles can deposit again near the apertures, forming new local clogging structures or reconstructing the original clogging structure (Fig. 15(c)). Consequently, the system develops a dynamic cyclic process involving temporary clogging, local breakthrough, and subsequent particle redeposition.

Overall, the evolution pathway of Type II mode can be described as: particle migration → local accumulation → temporary clogging → local hydraulic accumulation → breakthrough at weak locations → concentrated release → attenuation of hydraulic action → particle re-deposition. The essence of this sand-inrush mode lies in the dynamic competition between clogging reconstruction and particle release. When clogging reconstruction dominates, the clogging structure can reform after local breakthrough, causing particle migration and release to be restricted again. When particle release gradually becomes dominant, local breakthrough continues to expand and may further evolve into a stable and connected dominant seepage channel.



(a) Local accumulation and temporary clogging

(b) Hydraulic buildup and concentrated breakthrough

(c) Residual clogging, release weakening and re-clogging tendency

Fig. 15. Cyclic evolution mechanism of the Type II local clogging–staged release mode

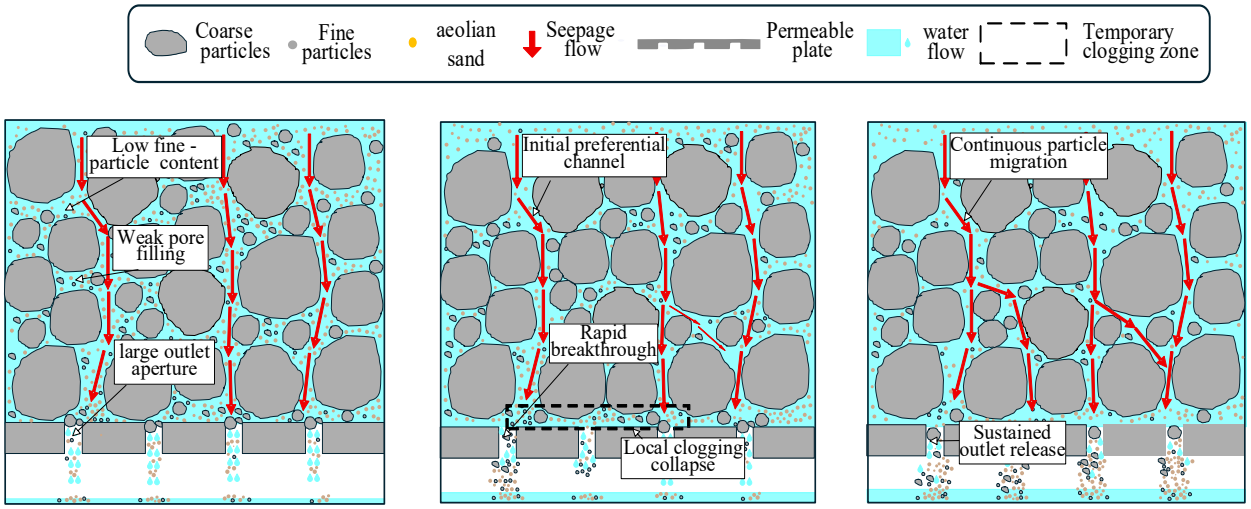
4.3 Positive-feedback evolution mechanism of Type III: channel breakthrough–sustained discharge mode

When the outlet release capacity is significantly higher than the local filling–clogging capacity, the broken rock mass exhibits the channel breakthrough–sustained discharge mode (Type III) of seepage-induced sand inrush (Fig. 16). Under this condition, the relatively low content of mudstone fine particles results in insufficient filling of the pore spaces within the coarse-particle skeleton. Consequently, the effective flow space inside the specimen is relatively large, and the pore connectivity is well developed. Although some migrating particles may still undergo temporary deposition near the permeable plate, the deposited layer and bridging structures formed are generally thin and have poor continuity due to insufficient fine-particle supply, making them difficult to maintain stably over a long period.

Once the local deposited structure near the outlet becomes unstable, water preferentially forms dominant seepage

channels along regions with lower resistance (Fig. 16(a)). Mudstone fine particles and upstream sand-source particles rapidly pass through these channels and continuously migrate out of the specimen with the water flow (Fig. 16(b)). With continuous particle loss, the pores surrounding the dominant channels gradually expand, reducing the seepage resistance of the channels. Consequently, water flow becomes increasingly concentrated within the dominant channels, which further enhances particle migration and promotes the additional release and loss of surrounding particles (Fig. 16(c)).

Overall, the evolution path of the Type III mode can be described as: weak pore filling → instability of local deposited structures → formation of dominant channels → continuous particle loss → pore-scale enlargement → reduction in channel resistance → enhanced seepage flow → continuous channel expansion. The essence of this sand-inrush mode lies in the continuous positive feedback between particle loss and seepage-channel expansion. This mechanism enables local breakthrough to progressively develop into stable connectivity of dominant channels, maintaining high seepage capacity and strong particle release intensity.



(a) Weak pore filling and early particle mobilization

(b) Unstable local accumulation and rapid breakthrough

(c) Preferential channel penetration and continuous particle discharge

Fig. 16. Positive feedback evolution mechanism of Type III: channel breakthrough–sustained discharge mode

In summary, the seepage-induced sand inrush response of broken rock masses is mainly governed by the relative dominance between local filling–clogging effects and outlet particle release capacity. When the clogging effect dominates, particle migration and release are suppressed, resulting in the Type I migration–deposition–clogging–slow-release mode. When the two effects compete with each other, local clogging repeatedly forms and becomes unstable, leading to the Type II local clogging–staged release mode. When the outlet release effect dominates, dominant seepage channels gradually develop and continuously expand, resulting in the Type III channel breakthrough–sustained discharge mode. With increasing Talbot exponent, the content of fine particles decreases, and the pore-filling and local clogging capacities gradually weaken. With increasing outlet aperture, the geometric constraints on particles passing through the outlet decrease, thereby enhancing particle release capacity. These two factors jointly alter the relative dominance between clogging and release, causing the seepage-induced sand inrush modes to generally evolve from stable local clogging to

staged breakthrough and then to sustained connectivity of dominant channels. The transition boundaries between different modes also vary with different combinations of particle gradation and outlet aperture.

From the perspective of shallow coal-seam mining, mining-induced disturbance can promote the gradual development of roof fracture zones and water-conducting fractures, while altering the outlet-scale conditions for particles from unconsolidated strata entering seepage channels. For broken media with a relatively high content of fine particles, local clogging can restrict particle migration and water–sand release during a certain stage. However, such clogging is strongly condition-dependent and does not imply long-term stability of roof water-sand migration pathways. With the expansion of mining-induced fractures, enlargement of effective flow scales, or continuous hydraulic disturbance to local clogging structures, the seepage-induced sand inrush response may gradually evolve from local clogging to staged release and sustained channel connectivity. Therefore, in the risk assessment of water–sand inrush in shallow coal seams, roof stability should not be evaluated solely on the basis of low initial water inflow or temporarily low sand content. Instead, the particle gradation of unconsolidated strata, the scale of seepage channels within fractured zones, and outlet boundary conditions should be comprehensively considered. For areas prone to local clogging, continuous variations in water pressure, water inflow, and sand content during mining should be closely monitored to prevent temporary clogging from masking potential channel instability risks. For areas exhibiting staged increases in flow and intermittent sand discharge, attention should be paid to sudden particle release caused by repeated failure of local clogging structures. When particle output continues to increase and shows clear channelized seepage characteristics, this may indicate that the water–sand migration channel has entered a rapid development stage. Under such conditions, the risk of water–sand inrush further increases, and these areas should be regarded as key targets for risk identification, prevention, and control.

4. Conclusions

Seepage-induced sand-inrush tests were conducted on broken rock masses using broken mudstone particles and aeolian sand as experimental materials under different combinations of particle gradation and permeable-plate aperture. The effects of the coupled interaction between particle gradation and outlet boundary conditions on equivalent permeability, sand-inrush characteristics, and response-mode evolution were analyzed. The main conclusions are as follows:

(1) As the Talbot exponent increased from 1.0 to 2.0 and the permeable-plate aperture increased from 1 to 5 mm, the equivalent permeability of all test conditions exhibits a nonlinear increasing trend. Under variations in Talbot exponent, the equivalent permeability increases by 46.3%–125.4% for different aperture groups. Under variations in permeable-plate aperture, the equivalent permeability increases by 106.4%–182.3% for different gradation groups.

(2) With increasing Talbot exponent from 1.0 to 2.0, the total sand discharge increases by 410.0%–1366.7% under different permeable-plate aperture conditions. With increasing permeable-plate aperture from 1 mm to 5 mm, the total sand discharge increases by 259.5%–994.5% under different Talbot gradation conditions. Meanwhile, the time to first sand emergence decreases for all test conditions with increasing Talbot exponent and permeable-plate aperture.

(3) Based on particle migration characteristics, outlet responses, and particle release processes, the seepage-induced sand inrush behavior of broken rock masses can be classified into three modes: Type I: migration–deposition–clogging–

slow-release mode, Type II: local clogging–staged release mode, and Type III: channel breakthrough–sustained discharge mode. These three modes correspond to the dominance of local filling–clogging effects, dynamic competition between clogging and release, and dominance of outlet release, respectively. Their macroscopic responses evolves from low permeability and low sand discharge, through staged release, to high-intensity sustained particle output.

(4) With increasing Talbot exponent, the content of mudstone fine particles smaller than 0.8 mm decreases, and the pore-filling and local clogging effects within broken rock masses are generally weakened. With increasing outlet aperture, the geometric constraints on particles passing through the outlet decrease, thereby enhancing particle release conditions. The combined effects of these two factors cause the seepage-induced sand inrush modes of broken rock masses to generally evolve from stable local clogging (Type I) to staged release (Type II) and finally to sustained connectivity of dominant channels (Type III).

Author contributions

Zhibin Lin: Writing - Review & Editing, Conceptualization, Methodology, Funding Acquisition. Zhaoyang Feng: Writing - Original Draft, Methodology, Investigation, Data Curation, Formal Analysis. Boyang Zhang: Writing - Review & Editing, Project Administration, Funding Acquisition. Yanchao Wang: Writing - Review & Editing, Validation.

Funding

This research was supported by the National Natural Science Foundation of China (Grant No. 52374087), the Natural Science Foundation General Project of Henan Province (Grant No. 262300421746).

Declarations

Conflict of interest The authors have the appropriate permission from responsible authorities to perform the study onsite and have no conflicts of interest.

Data availability

Data will be made available on request

References

W. Sui, Catastrophic mechanism of seepage deformation and failure of mining rock mass and its prevention & control I: Water-sand mixture inrush from seam roof, J. Earth Sci. Environ. 44 (6) (2022) 903–921, https://doi.org/10.19814/j.jese.2022.10001.

Q. Dong, H. Jia, M. Wei, W. Sui, J. Wang, C. Qing, H. Yang, G. Jin, Y. Liang, Risk mechanism of water and sand burst under the Neogene and thin bedrock: The influence of ancient erosion surface undulation and weathering degree, J. China Univ. Min. Technol. 53 (5) (2024) 889–900, https://doi.org/10.13247/j.cnki.jcumt.20240257

G. Zhang, R. Wang, J. Ma, W. Lyu, W. Zhang, H. Wang, Study on solid-fluid coupling similarity simulation test of water-sand inrush during mining of shallow buried thin bedrock roof, Coal Sci. Technol. 52 (6) (2024) 165–175, https://doi.org/10.12438/cst.2023-1227.

Y. Song, Water inrush and sand inrush mechanism and prevention technology during the initial mining period in 22402 working face of Halagou coal mine, Saf. Coal Mines 43 (12) (2012) 91–93, https://doi.org/10.13347/j.cnki.mkaq.2012.12.027.

Y. Xu, Z. Ma, X. Li, W. Miao, E. Zhang, W. Jiang, Y. Zhuo, Y. Tian, Research on the influence of the nature of the weathered bedrock zone on the roof water bursting and sand bursting: Taking Zhaogu No. 1 Mine as an example, Coal Sci. Technol. 51 (7) (2023) 64–71, https://doi.org/10.13199/j.cnki.cst.2021-1268.

F. Li, S. Yang, Z. Li, W. Yang, J. Yang, X. Chen, Experimental study on disaster of water-sand inrush and roof cutting in working face with thin bedrock roof, Coal Sci. Technol. 49 (11) (2021) 125–133, https://doi.org/10.13199/j.cnki.cst.2021.11.017.

B. Zhang, Y. Weng, Z. Li, Z. Lin, W. Wang, W. Song, H. Ren, Experimental research on the seepage characteristics of water-sand flow in crushed sandstone of the coal mine collapse-type water inrush and sand gushing, J. China Coal Soc. 50 (11) (2025) 5082–5093, https://doi.org/10.13225/j.cnki.jccs.2025.0905.

Z. Huang, Z. Wang, Q. Gu, X. Zhang, H. Xu, Y. Wu, Y. Lin, Characterizing seepage behavior of weakly cemented filling fault fracture zone, J. China Coal Soc. 50 (12) (2025) 5357–5369, https://doi.org/10.13225/j.cnki.jccs.2024.1381.

C. Huang, S. Zhang, Y. Gao, S. Wu, Y. Zhou, H. Sun, W. Wang, Q. Lu, Influence of particle loss on the seepage characteristics of tuff in the fault fracture zone under triaxial stress, Chin. J. Eng. 44 (7) (2022) 1134–1146, https://doi.org/10.13374/j.issn2095-9389.2021.11.22.001.

M. Xian, Z. Xu, B. Chen, Numerical investigation of variable-mass seepage mechanism of broken rock mass in faults, Comput. Geotech. 160 (2023) 105527, https://doi.org/10.1016/j.compgeo.2023.105527.

J. Yang, Z.-Y. Yin, F. Laouafa, P.-Y. Hicher, Analysis of suffusion in cohesionless soils with randomly distributed porosity and fines content, Comput. Geotech. 111 (2019) 157–171, https://doi.org/10.1016/j.compgeo.2019.03.011.

Y. Zhao, Z. Hu, Y. Zheng, Q. Wu, Influences of particle size ratio and fines content on the suffusion characteristics of gap-graded soils, Granul. Matter 26 (2) (2024) 52, https://doi.org/10.1007/s10035-024-01425-3.

M. Meng, S. Zhang, Z. Wei, J. Peng, X. Yang, H. Fan, Seepage behaviors of gap-graded sand subjected to suffusion, Bull. Eng. Geol. Environ. 84 (2) (2025) 101, https://doi.org/10.1007/s10064-024-04046-5.

D. Ma, H. Duan, W. Liu, X. Ma, M. Tao, Water-sediment two-phase flow inrush hazard in rock fractures of overburden strata during coal mining, Mine Water Environ. 39 (2) (2020) 308–319, https://doi.org/10.1007/s10230-020-00687-6.

B. Zhang, Q. He, Z. Lin, Z. Li, Experimental study on the flow behaviour of water-sand mixtures in fractured rock specimens, Int. J. Min. Sci. Technol. 31 (3) (2021) 377–385, https://doi.org/10.1016/j.ijmst.2020.09.001.

B. Chen, S. Zhang, Y. Li, J. Li, Experimental study on water and sand inrush of mining cracks in loose layers with different clay contents, Bull. Eng. Geol. Environ. 80 (1) (2021) 663–678, https://doi.org/10.1007/s10064-020-01941-5.

X. Xu, W. Sui, Water-sand mixture flow in single fractures and particle flow model modification based on effective aperture, Eng. Geol. 366 (2026) 108691, https://doi.org/10.1016/j.enggeo.2026.108691.

Y. Yin, Y. Cui, L. Jing, Clogging and unclogging of fine particles in porous media: Micromechanical insights from an analog pore system, Water Resour. Res. 60 (2024) e2023WR034628, https://doi.org/10.1029/2023WR034628.

H. Xiong, Z. Zhang, X. Sun, Z.-Y. Yin, X. Chen, Clogging effect of fines in seepage erosion by using CFD-DEM, Comput. Geotech. 152 (2022) 105013, https://doi.org/10.1016/j.compgeo.2022.105013.

J. Liang, W. Sui, M. Ye, S. Kasmaeeyazdi, F. Tinti, Water-sand mixture inrush in underground pathways: Risk factors and

mitigation strategies, Eng. Geol. 362 (2026) 108510, https://doi.org/10.1016/j.enggeo.2025.108510.

Z. Shen, Y. Zhao, Y. Lv, P. Wang, N. Hu, F. Shu, H. Gao, Z. Wang, Upward propagation of ground disturbance induced by water-sand inrush into a defective tunnel in a dual-stratum geological condition, Tunn. Undergr. Space Technol. 158 (2025) 106422, https://doi.org/10.1016/j.tust.2025.106422.

Y. Qin, N. Xu, Y. Guo, J. Li, W. Han, Physical simulation of the influence of the original rock strength on the compaction characteristics of caving rock in longwall goaf, R. Soc. Open Sci. 9 (9) (2022) 220558, https://doi.org/10.1098/rsos.220558.

P. Zhang, Y. Zhang, T. Zhao, Y. Tan, F. Yu, Experimental research on deformation characteristics of waste-rock material in underground backfill mining, Minerals 9 (2) (2019) 102, https://doi.org/10.3390/min9020102.

Y. Wu, Z. Huang, Q. Gu, Y. Lin, D. Moyo, Y. Wu, C. Zou, K. Zhao, Experimental investigation on the pore structure and water inrush evolution law of weakly cemented fault fracture zone with different filling gradations, Geomech. Geophys. Geo-Energy Geo-Resour. 9 (2023) 162, https://doi.org/10.1007/s40948-023-00705-1.

D. Ma, H. Duan, X. Li, Z. Li, Z. Zhou, T. Li, Effects of seepage-induced erosion on nonlinear hydraulic properties of broken red sandstones, Tunn. Undergr. Space Technol. 91 (2019) 102993, https://doi.org/10.1016/j.tust.2019.102993.

D. Ma, H. Bai, Z. Chen, H. Pu, Effect of particle mixture on seepage properties of crushed mudstones, Transp. Porous Media 108 (2) (2015) 257–277, https://doi.org/10.1007/s11242-015-0473-1.

Z. Lin, Y. Wang, B. Zhang, et al., Experimental study on critical hydraulic pressure gradient of sand inrush in broken rock mass, Coal Sci. Technol. (2026) 1–14, https://link.cnki.net/urlid/11.2402.TD.20260319.1354.007.

L. Zhang, S. Yang, H. Pan, T. Zhang, Permeability of broken coal around CBM drainage boreholes with the compound disaster of the rockburst and outburst, Appl. Sci. 15 (7) (2025) 3439, https://doi.org/10.3390/app15073439.

D. Ma, X.X. Miao, G.H. Jiang, H.B. Bai, Z.Q. Chen, An experimental investigation of permeability measurement of water flow in crushed rocks, Transp. Porous Media 105 (3) (2014) 571–595, https://doi.org/10.1007/s11242-014-0385-5.